

AD-A198 190

inal contains color
plates: All DTIC reproductions
will be in black and
white

DTIC FILE COPY

2

Shear-wave processing of sonic log waveforms in a limestone reservoir

DTIC
SELECTED
AUG 31 1988
E

David Goldberg* and William T. Gant†

ABSTRACT

Sonic full waveforms were recorded in a shale-limestone interval with an experimental 12-channel acoustic logging device. Well-defined shear (pseudo-Rayleigh) waves were observed throughout most of the 142 m interval and were used to distinguish lithologic boundaries and zones of fracturing as interpreted by acoustic borehole televiewer and standard geophysical logs. The high signal-to-noise ratio of the waveforms permitted meaningful shear velocities to be obtained by 12-fold semblance calculations in all but the washed-out intervals in this well. A correlation of changes in the V_p/V_s ratio with depth aided in identifying some compositional changes in the well, but such a correlation could not be used to distinguish fracturing in the limestone. Shear-wave amplitudes, however, were effective for identifying lithologic changes, as well as fractures, from the sonic log. Shear amplitudes were lower in the shale than in the limestone, and shear-wave attenuation increased in fractured zones. There was no strong correlation between the degree of fracturing and the attenuation of Stoneley waves. In general, shear-wave processing of sonic logs is recommended for interpretation of lithology and fracturing in any well in which full waveforms are recorded and shear waves propagate.

INTRODUCTION

In theoretical studies, the V_p/V_s ratio has been related to lithology, crack density, and pore-fluid saturation (O'Connell and Budiansky, 1974; Toksöz et al., 1976). These models generally predict that V_p/V_s will increase as the spatial crack density increases in a homogeneous medium, where the cracks are much smaller than the seismic wavelength. Laboratory investigations have also convincingly shown that the presence of flat cracks or pores in a homogeneous medium significantly re-

duces its elastic constants, and hence its seismic velocities (Birch, 1960; Nur and Simmons, 1969; Brace et al., 1972; Kuster and Toksöz, 1974; Mavko and Nur, 1979). Tatham (1982) suggests that the dependence of V_p/V_s on crack density is even stronger than on the elastic constants of the minerals comprising the matrix, but an association of crack density with lithology may enable a correlation between V_p/V_s and lithology. On the other hand, Wilkens et al. (1984) have shown, in laboratory measurements on limestone samples, a stronger dependence of V_p/V_s on carbonate content than on crack closure. Although the relative contributions of composition and microcracking on elastic properties are still uncertain, empirical relationships have commonly been applied to sonic logging data to interpret lithologic changes from V_p/V_s (Pickett, 1963; Nations, 1974; Kithias, 1976; Eastwood and Castagna, 1983). These applications are limited, however, because no unique relationships have been found (Moos and Zoback, 1983).

In this paper, the sonic waveform-derived V_p/V_s ratio is correlated with lithology and fracturing in a shale-limestone sequence. Considering the likelihood of nonunique results, we also investigate the amplitude and frequency of borehole wave modes as simple and sensitive indicators of changes in the borehole environment. Paillet and White (1982) fully discuss the theory of an acoustic wave's sensitivity to the borehole environment. In particular, relative changes in shear-wave amplitudes are largely dependent upon guided (pseudo-Rayleigh) waves in the borehole, and, as such, are affected by environmental features which are difficult to identify from traditionally processed sonic logs. The processing described in this paper is effective for the full-waveform data set of any sonic log in which shear waves propagate.

DATA

In this study, Schlumberger's experimental 12-channel sonic sonde was used to record acoustic waveforms from source depths of 1469.4 to 1327.4 m in a limestone-shale sequence in the Anadarko Basin, Oklahoma. The source is near the

Manuscript received by the Editor July 24, 1986; revised manuscript received October 21, 1987.

*Lamont-Doherty Borehole Research Group of Columbia University, Palisades, NY 10964.

†1015 Springbrook Drive, Plano, TX 75075.

© 1988 Society of Exploration Geophysicists. All rights reserved.

bottom of the sonde and 3.96 m below the nearest of a linear array of 12 equally spaced receivers spanning 1.68 m. The sonde was pulled upward at a constant rate from the bottom of the hole, and a set of waveforms was recorded for each source location at 15 cm depth intervals. The source generates an acoustic signal having a peak energy level in the 5 to 15 kHz frequency band (Kimball and Marzetta, 1984). The source was fired once for each receiver recording. Rapid firing of the source for the succession of 12 receivers resulted in a negligible change in source location during recording. Each waveform was digitized uphole at a 10 μ s sampling rate.

The compressional, shear, and Stoneley wave mode arrivals are prominent and are identified for waveforms recorded at the near receiver in Figure 1. The near-receiver waveforms have been compensated for low-frequency instrument biases and gain controlled to equalize the amplitude of late-arriving modes. Other geophysical logs recorded in this well are also displayed in Figure 1. The interpretation of these logs delineates a shale interval above 1393.3 m, a limestone interval below the shale to 1448.2 m, and a calcareous shale to the bottom of the well. Shale intervals generally have low induction and high gamma-ray readings, and in certain zones high caliper readings indicate the presence of washouts. In the limestone, neutron and density porosity measurements are relatively consistent, indicating good hole conditions, and the caliper log in this interval is constant, but 20 percent lower than in the shale.

Core descriptions in a nearby well support the identification of the shale, limestone, and calcareous shale intervals from the logs. The shales are highly interbedded and brecciated. Chert nodules are observed in layers up to 15 cm thick in the upper 10 m of the limestone, and extensive fracturing is observed throughout. These features are evident in an acoustic televiewer log in the limestone interval, where fractures intersecting the borehole appear as low-reflectance (dark) bands in the image (Figure 2). Near 1433.0 m, the observed fractures are presumably the largest in the logged interval and have a predominantly vertical orientation. The televiewer traveltime log, also shown in Figure 2, corresponds to the relative position of the televiewer to the borehole wall. The traveltime log shows the tool is slightly off center, but there is little ellipticity of the cylindrical hole, so that sonic waveform distortion caused by the ellipticity of the borehole is negligible.

DATA PROCESSING

Velocity analysis

In the past, semblance has been applied extensively to seismic reflection data to obtain stacking velocities. By adapting to the linear moveout of refraction data, multichannel sonic waveforms can be analyzed using semblance to obtain interval velocities. The semblance S_{ij} was described by Taner and Koehler (1969) as a measure of the coherence of multichannel

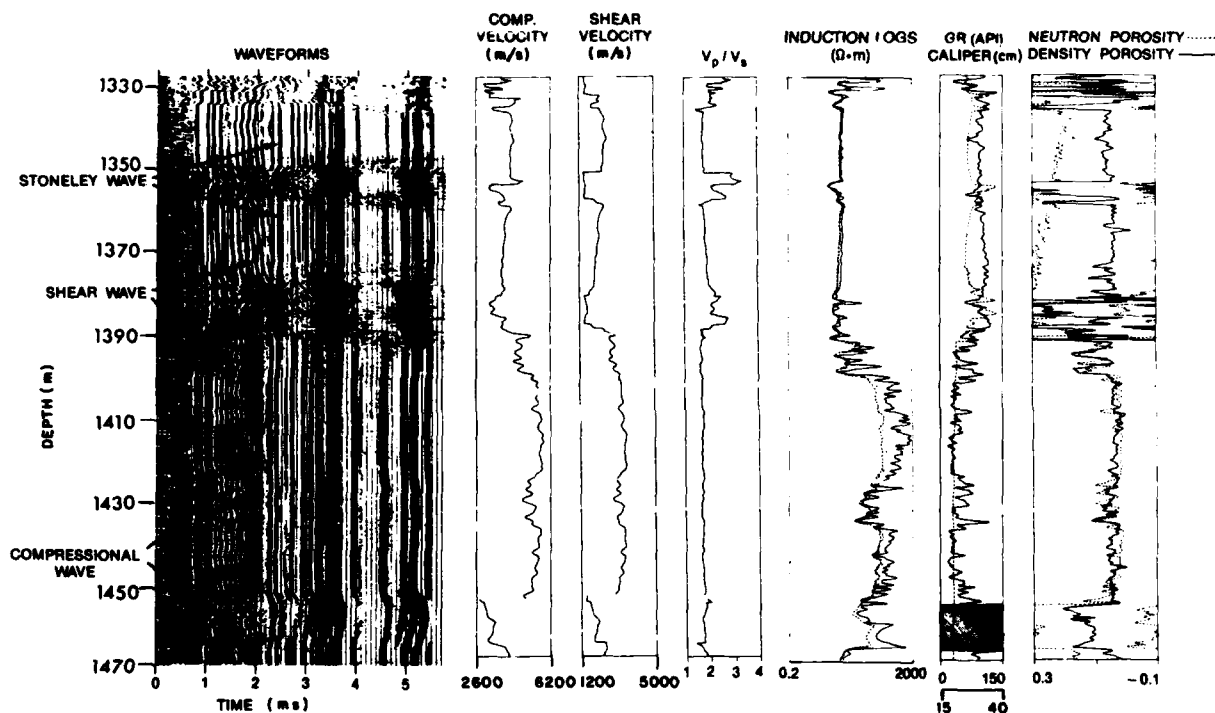


FIG. 1. Geophysical logs from 1327.4 to 1469.4 m depth. Gain-adjusted near-receiver waveforms, compressional and shear velocity logs, and V_p/V_s ; induction, gamma-ray, and caliper logs; and density (solid) and neutron (dashed) porosity curves. Three washouts of the borehole occur in the shale above 1393.3 m. From core analysis, chert layers were identified in the upper 10 m of the limestone and extensive fracturing occurs throughout. A porous calcareous shale underlies the limestone.

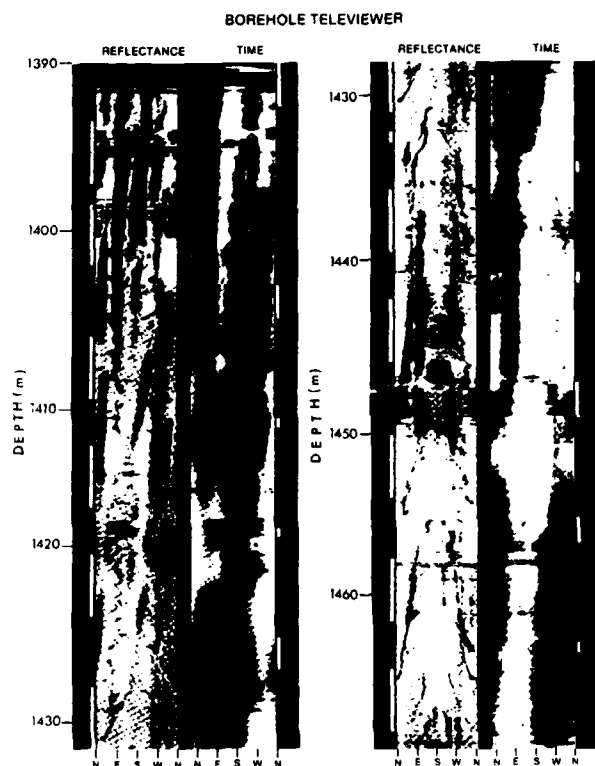


FIG. 2. Borehole televiewer reflectance and traveltime images in the limestone. Dark vertical banding indicates low reflectance due to intersecting fractures. The most intense fracturing occurs near 1433.0 m.

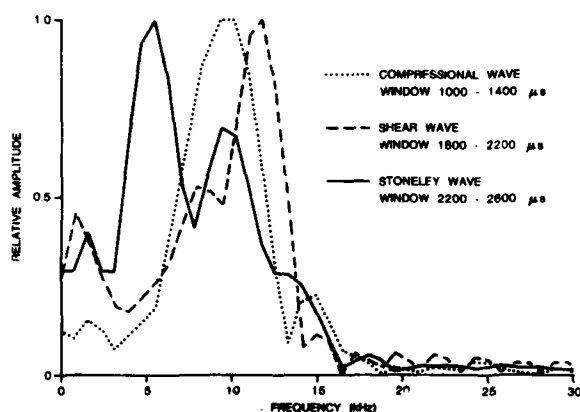


FIG. 3. Amplitude spectra of isolated compressional, shear, and Stoneley arrivals from a waveform recorded at 1469.4 m. Stoneley energy has significantly lower peak frequency than does either the compressional or shear energy.

signals, normalized by their autocorrelations at each time lag, and given by

$$\frac{\sum_{j=k-n}^{k+n} \left(\sum_{i=1}^M f_{ij} \right)^2}{\sum_{j=k-n}^{k+n} \sum_{i=1}^M (f_{ij}^2)}$$

where

M = the number of traces,

$n = 1/2N$,

N = the number of samples,

k = the center sample in the time window,

and

f_{ij} = the i th sample of the j th trace.

Semblance ranges between 0 and 1 for random and perfectly coherent signals, respectively, and can be used to calculate velocity by identifying the time lag at which the peak semblance value occurs. The time lag equals the receiver offset divided by the propagation velocity; the peak semblance value is directly related to the reliability of the calculation.

To enhance the accuracy of the semblance velocity measurements, time windowing, frequency filtering, and velocity filtering were used to remove interfering signals and noise for each individual wave mode. Figure 3 shows the bandwidths of amplitude spectra of time-windowed compressional, shear, and Stoneley arrivals. Since shear and compressional bands overlap, frequency filtering is not useful, but time windowing is generally adequate to isolate arrivals. The Stoneley spectral band is sufficiently different that band-pass filtering alone can separate Stoneley waves from interfering arrivals. The results of filter combinations are shown in Figure 4. A suite of gain-compensated waveforms recorded at a source depth of 1405.0 m are displayed on the left-hand side of the figure, and compressional, shear, and Stoneley arrivals, as identified by arrows, have progressively increasing moveout. The second suite from the left shows the application of a band-pass filter to discriminate against high-frequency and low-frequency noise and Stoneley-wave energy. A velocity filter is applied in the third suite to discriminate against high-velocity compressional energy. In the final suite, the combination of the band-pass and velocity filters used previously isolates low-velocity shear energy. Other combinations of filters can be designed to remove different signals or to isolate weak arrivals.

After processing to enhance the waveforms, compressional, shear, and Stoneley arrivals are isolated by picking the approximate start time of each arrival and using window lengths of approximately 1.5 periods. Semblance is then calculated and normalized to its maximum value. High-quality velocities with relatively high semblance were obtained over most of the logged interval for all three wave modes. The velocities and normalized semblance values are displayed for each mode in Figure 5. Summing of the semblance curves between adjacent depth points improves the stability of the velocity calculation, with some loss of resolution. However, the velocity resolution

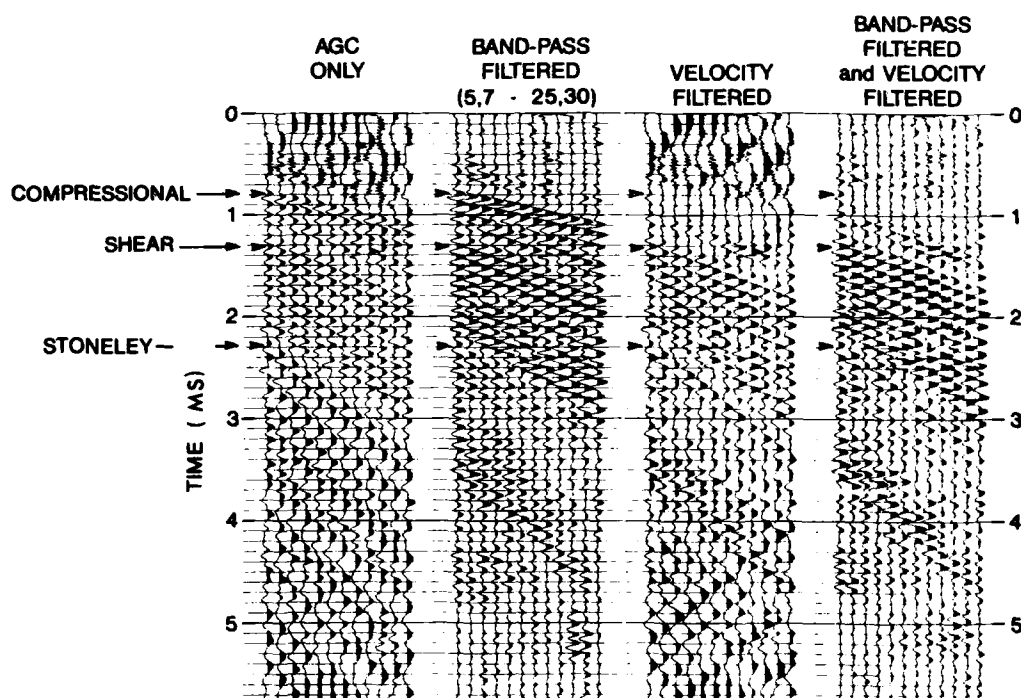


FIG. 4. Processed waveforms across the receiver array at a source depth of 1405.0 m. Waveforms are first gain-controlled and bias-compensated, then band-pass filtered to remove high-frequency and low-frequency noise and to separate the Stoneley energy, velocity-filtered to remove compressional energy, and finally band-pass and velocity filtered to isolate shear energy.

for thin beds is not significantly affected if the summing operator is shorter than the receiver span. For these displays, the semblance is summed over 0.76 m intervals. The resulting semblance is low for all wave modes only in the washed-out intervals between 1390.2 and 1375.0 m, 1359.8 and 1347.6 m, and 1333.8 and 1327.4 m (Figure 5). In those zones, fluid, shear, and Stoneley velocities are all near 1500 m/s, so that their arrivals interfere with each other and result in low semblance. Frequency and velocity filtering to separate these arrivals did not effectively increase the quality of the calculated velocities. The irregular shape of the borehole in these zones may be a major contributing factor to the difficulty in separating wave modes.

Figure 6 illustrates waveforms recorded across a sharp shale-limestone boundary. Low-amplitude compressional waves are not visible to the eye at this plotting scale. Shear-wave move-out dramatically decreases as the receiver array progresses across the velocity contrast and from left to right across the figure. Shear velocity increases by about 1000 m/s across the boundary, and because the velocity difference is large, a semblance peak is calculated corresponding to the velocity on each side. The layer having more receivers will have higher peak semblance. In the case of narrower velocity differences between layers, semblance correlation results in averaging of the velocities over the receiver span.

Amplitude analysis

Amplitudes of the waveforms were calculated by two different methods. In the first method, a time-domain measure of

amplitude, the amplitude envelope was calculated using $E(t) = [f^2(t) + f_H^2(t)]^{1/2}$, where $f_H(t)$ equals the Hilbert transform of $f(t)$ (Bracewell, 1965). The computed amplitude envelope is shown in color in Figure 7 for near-receiver and far-receiver waveforms. The vertical axis corresponds to depth in the well, and the 1.68 m offset between near and far receivers is not aligned in order to maintain a common source location for each depth point. The time scale is truncated to exclude the high-amplitude Stoneley arrival from scaling. Compressional and shear attenuation is apparent by a loss of amplitude between near and far receivers. Attenuation is greatest for shear waves near 1433.0 m, where losses up to 70 percent occur across the array, although elsewhere, shear attenuation is about 50 percent across the array. The variation of the amplitude envelope over the interval suggests a correlation between attenuation and lithology, fracturing, and borehole conditions.

The second measure of amplitude is derived from the cross-power spectrum of the near-receiver and far-receiver waveforms. The crosspower spectrum can be calculated by the Fourier transform of the crosscorrelation of time signals (Robinson and Treitel, 1980). The crosscorrelation of signals $x(t)$ and $y(t)$ is defined by

$$r_{xy}(k) = \lim_{T \rightarrow \infty} \frac{1}{2T+1} \sum_{k=-T}^T x(t+k)y(t),$$

where T is the number of time samples, and k is the time lag. The Fourier transform of $r_{xy}(k)$ may be expressed as

$$R_{xy}(\omega) = \int_{-\infty}^{\infty} r_{xy}(k)e^{-i\omega k} dk.$$

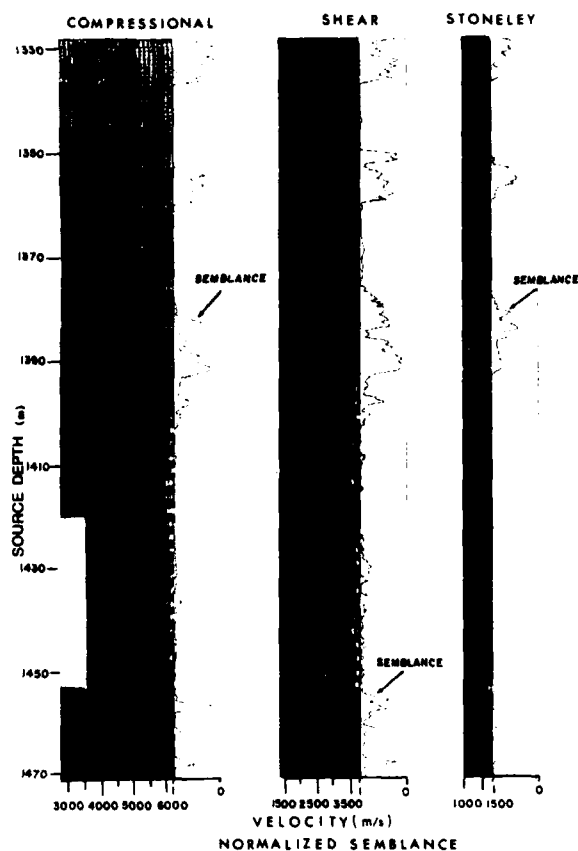


FIG. 5. Calculated velocities, normalized semblance, and time picks of isolated compressional, shear, and Stoneley wave-mode arrivals. Semblance is summed over 0.76 m intervals to improve the stability of the velocity calculation. Low semblance occurs in washouts and at severe velocity contrasts.

Peak magnitude and frequency are calculated from $R_{xy}(\omega)$ in order to correlate better sonic amplitude and frequency data with lithology, fracturing, and borehole conditions. These results are discussed below.

RESULTS

The V_p/V_s ratio

In Figure 8, the results of compressional and shear velocity analyses have been crossplotted and grouped for detailed lithologic interpretation by a depth correlation between the crossplot and the logs. The slope of the data in the crossplot represents the V_p/V_s ratio and varies between about 1.50 and 2.0 over the interval. Subgroupings of the data labeled A through J illustrate, for example, that washout intervals (J) have constant shear velocities equal to the fluid velocity (1500 m/s), and therefore data from those intervals are believed to be unreliable. Compressional and shear velocities are greater by about 1000 m/s in the limestone (F, G, H, and I) than in the shale (B, C, and E), although the V_p/V_s value is lower in the shale. The fractured (G) and chert interbedding (F) intervals have lower velocities than the surrounding limestone, although V_p/V_s remains relatively unchanged. In addition, the V_p/V_s ratio is not constant within the shale (B and C) and calcareous shale (A and D) intervals. Hence, the V_p/V_s ratio is effective for distinguishing major lithologic changes, but is unreliable in washouts, and cannot be used to discriminate between fractured and unfractured intervals in this well.

Crosspower spectra

The peak magnitudes of the crosspower spectra from isolated compressional, shear, and Stoneley wave modes are plot-

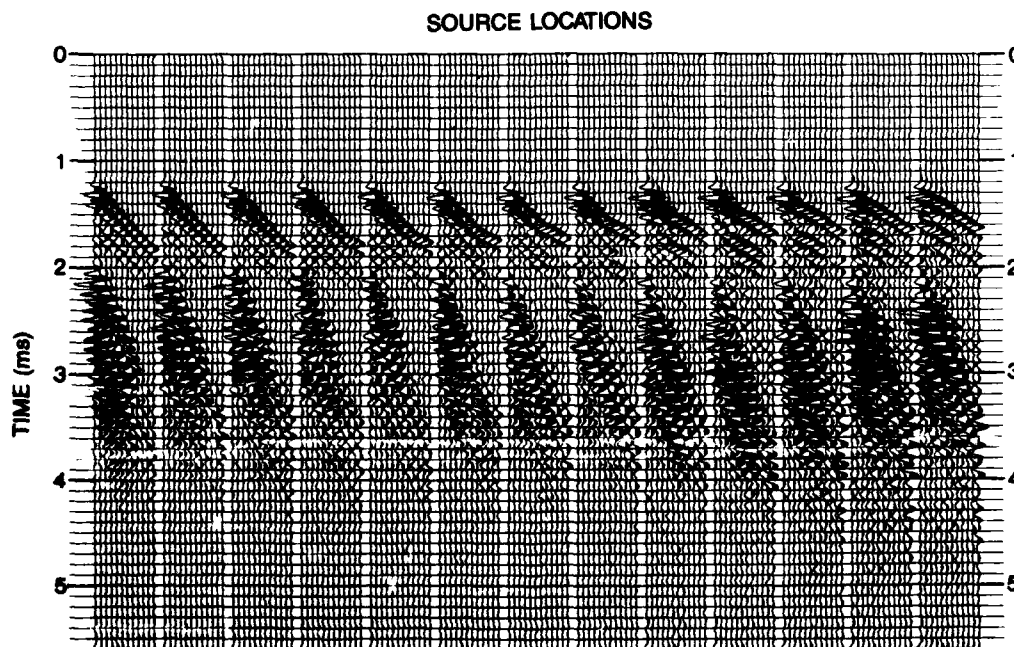


FIG. 6. Unprocessed waveforms recorded at each receiver for 15 cm incremental source depths from left to right across a shale-limestone boundary. Shear and Stoneley moveouts decrease progressively as more receivers move into the limestone. Low-amplitude compressional arrivals are not visible to the eye.

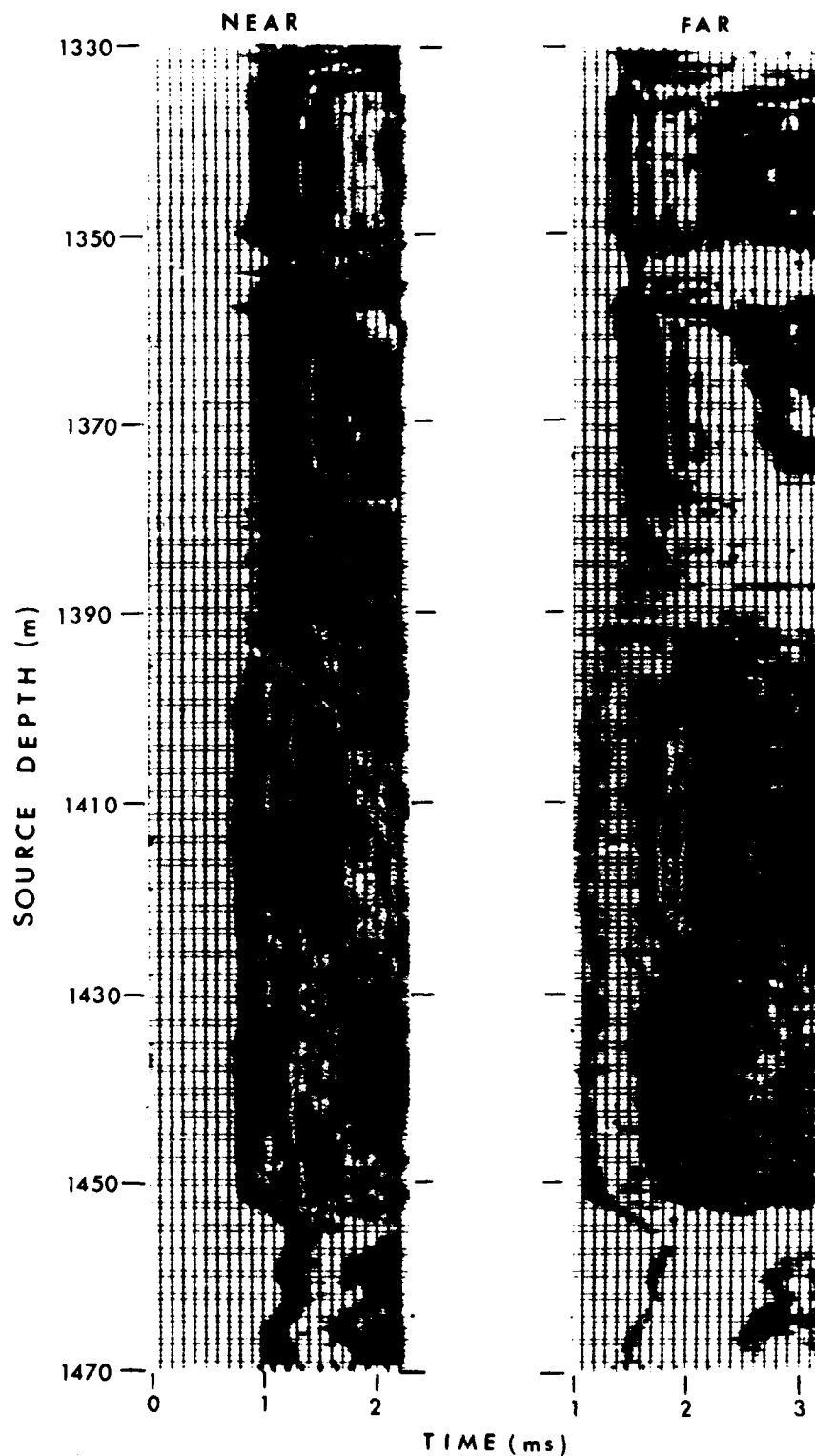


FIG. 7. Amplitude envelope color display for near-receiver and far-receiver waveforms at every fourth source location. The color scale illustrates the relative variation in amplitude across the receiver array and with depth.

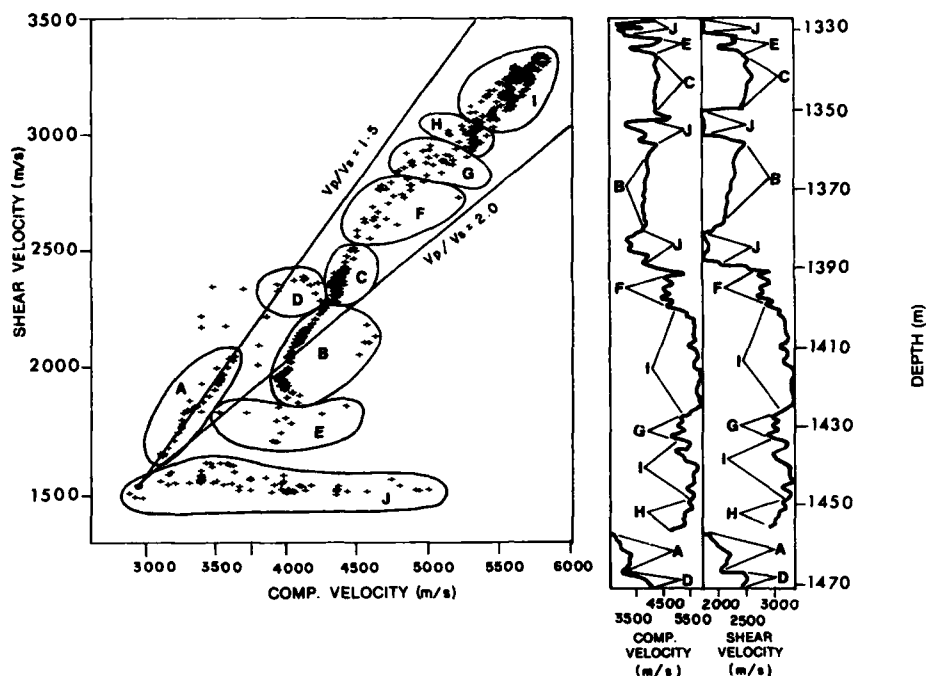


FIG. 8. Crossplot of V_p and V_s , where data have been grouped corresponding to their depth intervals. Shale (B and C), calcareous shale (A and D), and limestone (F, G, H, and I) intervals are distinguishable. Washouts (J) show a constant shear velocity (1500 m/s) which is unreliable. Chert interbedding (F) and fracturing (G) in the limestone are distinguished by decreases in velocity, although the V_p/V_s ratio remains unchanged.

ted as a function of depth in Figure 9. The caliper log, which measures the diameter of the borehole, is also displayed. The compressional amplitude is high in the shale and low in the limestone and calcareous shale. Note that large decreases in shear amplitude occur in the fractured interval near 1433.0 m and at the sharp shale-limestone boundary at 1457.3 m, where there are no significant changes in the borehole's diameter. The decay of the shear amplitude in these zones is clearly associated with these features. In the overlying shale, however, low shear amplitudes may be due to both poorer shear-wave propagation and a larger borehole diameter than in the limestone. The lowest shear amplitudes recorded in the well occur in the shale.

Both shear and Stoneley amplitudes typically decrease in fractured intervals (Paillet, 1980; 1981), although in this well, only shear amplitudes appear to be affected. Stoneley amplitudes decrease in washouts and at the sharp shale-limestone boundary and are relatively unaffected by fracturing or the decrease in the diameter of the borehole in the limestone. This insensitivity to fracturing and borehole size may be due to amplifier saturation during recording of the high-amplitude Stoneley wave.

The peak frequencies of isolated compressional, shear, and Stoneley wave modes are also plotted in Figure 9. Compressional and shear peak frequencies are nearly equal and decrease from about 9 kHz in the limestone to about 7 kHz in the shale. Because the frequency contents of compressional and shear waves are governed largely by the resonant frequency of guided waves in the borehole, any variation in the peak frequency can be attributed primarily to changes in the size of the borehole (Paillet and White, 1982). Stoneley-wave frequencies remain constant over the well, which may also be

a result of recording saturation. We place lower confidence in the frequency measurements in washouts, however, since compressional, shear, and Stoneley arrivals are all severely attenuated.

DISCUSSION

In this well, the relationship between the lithology and V_p/V_s values calculated from the sonic logs is not unique, since V_p/V_s values alone cannot distinguish all of the environmental and lithologic changes. For example, thin chert layers and fractures in the limestone affect the velocities in such a way that V_p/V_s remains unchanged from that of the surrounding rock, but both V_p and V_s individually decrease in a similar manner. A theoretical dependence of V_p/V_s on microcracks and lithology in homogeneous media will be invalid if inhomogeneities are present which have a spatial distribution similar to the sonic wavelength, which may explain the fact that V_p/V_s is apparently constant throughout the limestone. Localized alteration in crystalline rock may possibly explain increases in V_p/V_s near fractures (Moos and Zoback, 1983), which implies that little alteration has occurred in this well or that the effect of partially altered or open fractures compensates for any change in V_p/V_s due to alteration. As a result, the V_p/V_s ratio and fracturing in this well are difficult to correlate. These velocity measurements in fractured limestone suggest that compositional and structural effects on elastic properties are complicated and cannot be explained by existing theories or simple empirical models.

However, the amplitudes of sonic waves, which are dominated by guided-wave modes, are more sensitive than veloci-

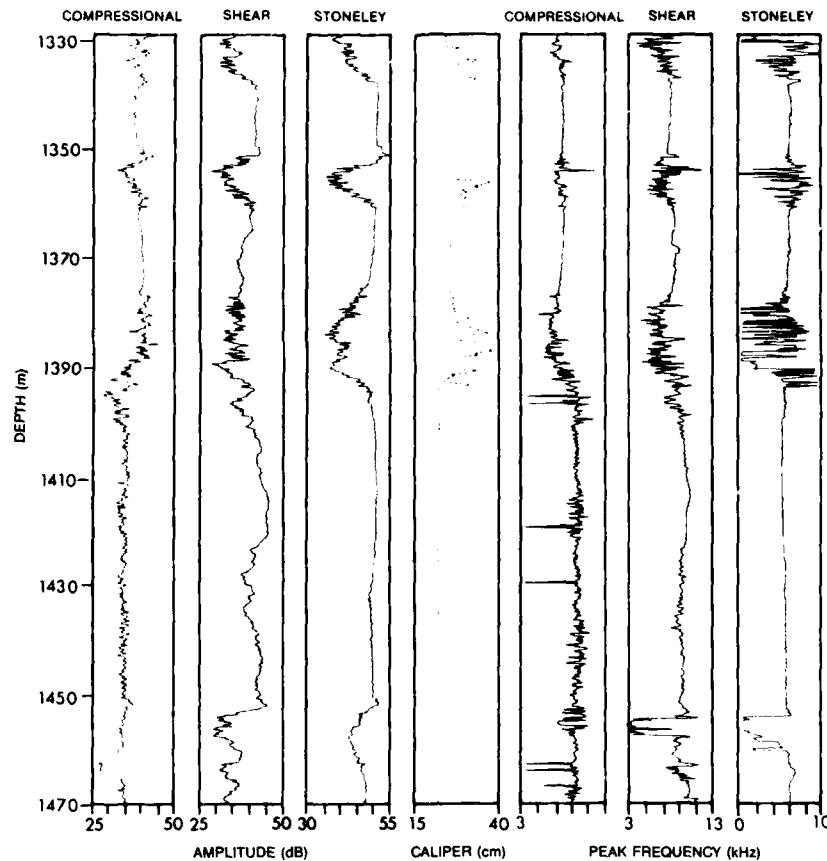


FIG. 9. Crosspower magnitude and peak frequency of isolated wave modes and the borehole caliper log. Shear amplitude is attenuated in the shale and in the fractured zone of the limestone. Stoneley-wave attenuation occurs in washouts, but shows little response to the decreasing borehole radius or to fracturing in the limestone.

ties to fracturing and environmental changes in this well. Below 1400 m, the apparent shear-wave attenuation can be attributed to the fractured zone and the calcareous shale boundary, where the borehole's diameter is constant. In the shale, shear-wave attenuation is greater than in the limestone, but the varying borehole diameter precludes a clear distinction between geometric and lithologic effects. Poor transmission of energy across bedding planes (as typically occurs in shale), fracturing, local changes in pore fluid content, and late-arriving reflections from sharp boundaries may all reduce shear amplitudes, but such factors are only separable from geometric effects if the size of the borehole is constant. Apparent shear-wave attenuation in inhomogeneous formations may therefore result from several different mechanisms. Nonetheless, using traditional sonic tools and simple processing of sonic waveforms, shear-wave amplitudes may aid in identifying lithologic and structural features at small expense.

SUMMARY

In this case study, borehole wave-mode velocities were calculated with high accuracy by a semblance algorithm. Wave-mode isolation increased the semblance and improved the ve-

locity calculation. In washouts, shear energy is difficult to isolate due to the coincidence of shear, fluid, and Stoneley arrivals, and the calculated shear velocity is unreliable. The V_p/V_s ratio is greater in the shale than in the limestone and calcareous shale. Near-vertical fracturing in the limestone does not significantly change the V_p/V_s value, though both V_p and V_s decrease in a similar manner, probably due to a combination of fracturing and alteration effects on the sonic velocities.

Sonic amplitudes were also calculated and correlated with lithologic and environmental changes. The limestone exhibits lower compressional-wave amplitude and higher shear-wave amplitude than the shale, and both compressional and shear frequencies are higher in the limestone than in the shale, primarily due to a decrease in the borehole's diameter. Stoneley-wave amplitude is nearly constant in both lithologies, even though there are significant changes in the diameter of the borehole, and all the wave modes are severely attenuated in washouts. In the limestone interval, where the effect of the borehole is constant, the shear amplitude log is the most effective tool for distinguishing lithologic boundaries and zones of fracturing. In the shale, where the borehole's diameter is not constant, the variable geometric effects must be removed in order for the observed changes in amplitude and frequency content to be attributed uniquely to lithologic variations.

ACKNOWLEDGMENTS

We would like to thank ARCO Resources Technology for permission to release the geophysical and geologic data. The core geology was described by W. Belfield, and the borehole televiewer data was supplied by R. Siegfried. Consultations on programming with C. Parker, J. Crowley, B. Black, and D. Lafferty and on the manuscript with D. Moos and J. Castagna are greatly appreciated. Lamont-Doherty Geological Observatory contribution number 4217.

This research was partially supported by the U.S. National Science Foundation grant no. JOI 66-84 and the Office of Naval Research grant no. N00014-87-K-0204.

REFERENCES

- Birch, F., 1960. The velocity of compressional waves in rocks to 10 kilobars, Part I: *J. Geophys. Res.*, **65**, 1083-1102.
- Brace, W. F., Silver, E., Hadley, K., and Goetz, C., 1972. Cracks and pores: a closer look: *Science*, **178**, 162-164.
- Bracewell, R., 1965. The Fourier transform and its applications: McGraw-Hill Book Co.
- Eastwood, R., and Castagna, J. P., 1983. Basic for interpretation of V_p , V_s in complex lithologies: *Trans., Soc. Prof. Well-log Anal. Logging Sympos.*, paper NN.
- Kithias, B. A., 1976. Lithology, gas detection, and rock properties from acoustic logging system: *Trans., Soc. Prof. Well-log Anal. Logging Sympos.*, paper R.
- Kimball, C. V., and Marzetta, T. L., 1984. Semblance processing of borehole acoustic array data: *Geophysics*, **49**, 274-281.
- Kuster, C. V., and Toksöz, M. N., 1974. Velocity and attenuation of seismic wave in two-phase media: Part II—Experimental results: *Geophysics*, **39**, 607-618.
- Mavko, G. M., and Nur, A., 1979. Wave attenuation in partially saturated rocks: *Geophysics*, **44**, 161-178.
- Moos, D., and Zuback, M. D., 1983. In situ studies of velocities in fractured crystalline rocks: *J. Geophys. Res.*, **88**, 2345-2358.
- Nations, J. F., 1974. Lithology and porosity from acoustic shear and compressional wave transit-time relationships: *Trans., Soc. Prof. Well-log Anal. Logging Sympos.*, paper Q.
- Nur, A., and Simmons, G., 1969. The effect of saturation on velocity in low porosity rocks: *Earth and Plan. Sci. Lett.*, **7**, 183-193.
- O'Connell, R. J., and Budiansky, B., 1974. Seismic velocities in dry and saturated cracked solids: *J. Geophys. Res.*, **77**, 5412-5426.
- Paillet, F. L., 1980. Acoustic propagation in the vicinity of fractures which intersect a fluid filled borehole: *Trans., Soc. Prof. Well-log Anal. Logging Sympos.*, paper DD.
- , 1981. A comparison of fracture characterization techniques applied to near-vertical fractures in a limestone reservoir: *Trans., Soc. Prof. Well-log Anal. Logging Sympos.*, paper XX.
- Paillet, F. L., and White, J. E., 1982. Acoustic modes of propagation in the borehole and their relationship to rock properties: *Geophysics*, **47**, 1215-1228.
- Pickett, G. R., 1963. Acoustic character logs and their application in formation evaluation: *J. Petr. Tech.*, **15**, 659-667.
- Robinson, E., and Treitel, S., 1980. Geophysical signal analysis: Prentice-Hall, 213-225.
- Taner, M., and Koehler, F., 1969. Velocity spectra—Digital computer derivation and applications of velocity functions: *Geophysics*, **34**, 859-881.
- Tatham, R. H., 1982. V_p , V_s and lithology: *Geophysics*, **47**, 336-344.
- Toksöz, M. N., Cheng, C. H., and Timur, A., 1976. Velocities of seismic waves in porous rocks: *Geophysics*, **41**, 621-645.
- White, J. E., and Zechman, R. E., 1968. Computed response of an acoustic logging tool: *Geophysics*, **33**, 302-310.
- Wilkins, R. H., Simmons, G., and Caruso, L., 1984. The ratio V_p/V_s as a discriminant of composition for siliceous limestones: *Geophysics*, **49**, 1850-1860.

Accession For	
NTIS GRA&I	<input checked="" type="checkbox"/>
DTIC TAB	<input type="checkbox"/>
Unannounced	<input type="checkbox"/>
Justification	
By	
Distribution/	
Availability Codes	
Dist	Avail and/or Special
A-1	21

